Localized optical- quality doping of graphene on silicon waveguides through a TFSA-containing polymer matrix

Misseeuw, Lara Renée; Ciuk, Tymoteusz; Krajewska, Aleksandra; Pasternak, Iwona; Strupinski, Wlodek; Feigel, Benjamin; Khoder, Mulham; Vandriessche, Isabelle; Van Erps, Jürgen; Van Vlierberghe, Sandra; Thienpont, Hugo; Dubruel, Peter; Vermeulen, Nathalie

Published in:
Journal of Materials Chemistry C

DOI:
10.1039/c8tc03198c

Publication date:
2018

Journal of
Materials Chemistry C

Accepted Manuscript

This article can be cited before page numbers have been issued, to do this please use: L. Misseeuw, T. Ciuk, A. Krajewska, I. Pasternak, W. Strupinski, B. Feigel, M. Khoder, I. Van Driessche, J. Van Erps, S. Van Vlierberghe, H. Thienpont, P. Dubruel and N. Vermeulen, *J. Mater. Chem. C*, 2018, DOI: 10.1039/C8TC03198C.

ROYAL SOCIETY OF CHEMISTRY

rsc.li/materials-c

View Article Online
DOI: 10.1039/C8TC03198C

Localized optical-quality doping of graphene on silicon waveguides through a TFSA-containing polymer matrix

Lara Misseeuw[a*], *Tymoteusz Ciuk*[b], *Aleksandra Krajewska*[b,c], *Iwona Pasternak*[b,d], *Wlodek Strupinski*[b,d], *Benjamin Feigel*[a], *Mulham Khoder*[a], *Isabelle Vandriessche*[e], *Jürgen Van Erps*[a], *Sandra Van Vlierberghe*[a,f], *Hugo Thienpont*[a], *Peter Dubruel*[f], *Nathalie Vermeulen*[a]

a. Brussels photonics team (B-PHOT), Dept. of Applied Physics and Photonics (IR-TONA), Vrije Universiteit Brussel, Pleinlaan 2, B-1050 Brussels, Belgium

*lmisseeu@b-phot.org

b. Institute of electronic materials technology, Wolczynska 133, 01-919 Warsaw, Poland

c. Institute of optoelectronics, Military University of Technology, Gen. S. Kaliskiego 2, 00-908 Warsaw, Poland

d. Faculty of Physics, Warsaw University of Technology, Koszykowa 75, 00-662 Warsaw, Poland

e. Sol-gel centre for research on inorganic powders and thin films synthesis, Ghent University, Krijgslaan 281 (S3), B-9000 Ghent, Belgium

f. Polymer Chemistry & Biomaterials research group, Ghent University, Krijgslaan 281 (S4 Bis), B-9000 Ghent, Belgium

View Article Online
DOI: 10.1039/C8TC03198C

Abstract

The use of graphene in optical and photonic applications has gained much attention in recent years. To maximize the exploitation of graphene's extraordinary optical properties, precise control over its Fermi level (e.g. by means of chemical doping) will be of vital importance. In this work, we show the usage of a versatile p-doping strategy based on the incorporation of bis(trifluoromethanesulfonyl)amide (TFSA), functioning as active p-dopant molecule, into a poly(2,2,3,3,4,4,5,5-octafluoropentyl methacrylate) (POFPMA) polymer matrix. The TFSA/POFPMA dopant can be utilized both onto large size graphene regions via spin coating and on small predefined spatial zones of micrometer dimension by localized inkjet printing. Whereas pure TFSA suffers from a clustered layer deposition combined with environmental instability, the application of the POFPMA polymer matrix yields doping layers revealing superior properties counteracting the existing shortcomings of pure TFSA. A first key finding relates to the optical quality of the dopant layer. We obtain a layer with an extremely low surface roughness (0.4-0.8 nm/25 μm^2) while exhibiting very high transparency (absorbance < 0.05%) over the 500-1900 nm wavelength range, with strongly enhanced doping stability as a function of time up to several weeks (for inkjet-printed deposition) and months (for spin coated deposition). Finally, the doping efficiency is very high, reaching a carrier density around +4 x 10^{13} cm^{-2} whereas the optical transmission of a graphene-covered Si waveguide revealed a strong improvement (4.22 dB transmission increase per 100 µm graphene length at the wavelength of 1550 nm) after deposition of the dopant via inkjet printing.

1. Introduction

Ever since graphene was isolated in 2004 [1], it has been the subject of breakthrough research due to its outstanding and unique physical properties [2]. The two-dimensional material consisting of sp^2-hybridized carbon atoms organized into a honeycomb lattice, exhibits extraordinary electrical characteristics (i.e. high electron mobility [3] at room temperature ($\mu = 2 \times 10^5$ cm^2 V^{-1} s^{-1})) and exceptional mechanical robustness (intrinsic strength and elasticity of σ_{int} = 130 GPa and E = 1 TPa, respectively [4]).

In addition, graphene is also characterized by specific optical properties. As a result, graphene can be integrated into a variety of photonic applications [5]. Indeed, pristine

View Article Online
DOI: 10.1039/C8TC03198C

graphene exhibits a strong linear optical absorbance of 2.3% per layer, independent of the wavelength [6] and mainly caused by interband transitions [7]. Furthermore, it is known that graphene features a very strong nonlinear response [8]. Hendry *et al.*[9] determined the Kerr susceptibility of graphene ($\chi^{(3)}$) to be 10^{-7} esu (electrostatic units) using four-wave mixing (FWM). Recently, the Kerr nonlinearity of graphene on a silicon waveguide was measured by chirped-pulse-pumped self-phase modulation (SPM) [10], which yielded the same magnitude as measured by Hendry *et al.* and additionally, revealed a negative nonlinearity sign. Earlier this year, our group showed that rather than the nonlinear susceptibility, a complex saturable refraction process is central to graphene's SPM behavior [11]. Covering an optical waveguide with graphene results in an interaction between the evanescent tails of the guided light through the waveguide and the deposited graphene monolayer. As a result, the performance of a photonic chip will change significantly both in terms of optical losses (due to the strong linear absorbance of graphene [12,13]) as well as nonlinear behavior (due to the strong nonlinearity of graphene [10,11]). As a result, the improved nonlinear optical functionality of graphene deposited onto a waveguide-based photonic device can play an important role in the development of on-chip nonlinear-optical light sources [13,14]. However, the output power of the chip decreases drastically with the increasing length of the graphene-covered waveguide due to graphene's strong absorbance.

Another remarkable property of graphene is the ability to tailor its electronic and optical characteristics by shifting graphene's Fermi level. The position of the Fermi level is dependent on the type and concentration charge carriers in graphene, which can be altered by graphene doping. The applied dopant strategy is able to either extract electrons from graphene (p-type doping, resulting in a shift of the Fermi level below the Dirac point) or donate electrons to graphene (n-type doping, resulting in a shift of the Fermi level above the Dirac point). However, for most optical applications of graphene, only the magnitude of the graphene Fermi level is important rather than its sign [15]. Indeed, for both n- and p-type doping, the linear optical absorbance will be lower as a consequence of suppressed interband transitions, which is a necessity for graphene's optical usability.

One way to shift the Fermi level is via electrical gating; by applying a gate voltage onto a dielectric or electrolyte in contact with graphene, the position of the Fermi level can be precisely tuned from conduction to valence band [16]. Another common approach to control the carrier type and density in graphene is based on chemical doping [17], a technique which

View Article Online
DOI: 10.1039/C8TC03198C

can be subdivided in substitutional doping (several carbon atoms in the graphene layer are replaced by an atom with a different number of valence electrons) and surface transfer doping (dopant molecules are adsorbed onto the graphene surface to induce an electron exchange between graphene and the adsorbed layer). A last, but less frequently applied doping approach, classified within chemical doping, is based on covalent functionalization of graphene. This can be achieved for example by treatment with chlorine plasma [18] or electron beam lithography [19].

Whereas electrical gating of graphene is flexible and tunable upon changing the gate voltage, chemical doping offers a permanent doping level depending on the dopant strength and applied dopant concentration [20]. Although the former results in very promising doping efficiencies (n ranging from -3×10^{13} cm^{-2} to $+4 \times 10^{13}$ cm^{-2}, with n being charge carrier concentration [21]), it requires advanced nanofabrication techniques for positioning electrical contacts and the usage of a voltage source [22], which is not always desirable, nor possible. Additionally, a noteworthy hysteresis effect is observed upon gating graphene with electrolytes [23]. Consequently, chemical doping will be our main focus for controlling graphene's Fermi level. Because substitutional doping and covalent functionalization lead to invasive alterations of graphene's crystalline structure with subsequently deteriorated carrier mobility and conductivity [24], we select the surface transfer approach as the most promising one for graphene doping towards optical applications.

Chemical doping of graphene for optical applications needs to comply with essential requirements in order to maintain graphene's unprecedented qualities in the optical application domain. First, the method needs to be efficient and stable over time. Secondly, the applied dopant layer needs to be of high optical quality, i.e. it should be highly transparent (light absorption < 0.05%, for every applied layer regardless its thickness, in the visible, near and mid-infrared, because this includes the region of interest for many on-chip optical applications) with a low surface roughness (root mean square (RMS) roughness < 5 nm or an optical quality of $\lambda/200$ at λ = 1000 nm over a surface of 25 μm^2) to avoid additional optical light scattering when light passes through the doped graphene. Finally, the doping strategy should be preferably straightforward to apply.

Graphene, grown on copper and transferred on the desired substrates, already features unintentional p-type doping as a consequence of air exposure and PMMA residues associated with the graphene transfer [25,26]. Consequently, the present work focusses on a

View Article Online
DOI: 10.1039/C8TC03198C

strategy to further increase the p-doping efficiency. Therefore, when looking at surface transfer doping, strong electron acceptor molecules will have to be applied to extract electrons from graphene, thereby further lowering its chemical potential. This can be achieved by using different dopant molecules, including inorganic acids [27,28] (H_2SO_4, HNO_3, HCl, $HAuCl_3$), transition metal oxides (MoO_3 [29,30] and VO_x [31]), strong organic π-electron acceptors (e.g. F4-TCNQ [32]), organic acids (TFSA [33–35] and TFMS [36]) and metal chlorides [37–39] ($AuCl_3$,, $RhCl_3$ and $FeCl_3$). However, to the best of our knowledge, the chemical doping methods reported so far, do not fulfill the requirements in terms of optical quality due to a rough surface [38,40,41] and corresponding optical loss of at least 1% for light passing perpendicularly through the graphene sheet [35,41,42] In addition, some of the applied dopant layers suffer from poor stability due to time-dependent desorption of adsorbed dopants [43,44]. Recently, another approach towards surface transfer doping was developed, namely photoinduced charge transfer [22,45–47]. The latter technique however requires back-gated sample design [46] and a controlled atmosphere by continuous illumination [22], which cannot, to the best of our knowledge, be considered as easily applicable in future optical applications. We recently reported on a new p-type doping strategy with optical quality, based on a spin coated F4-TCNQ/MEK layer [48]. In that work, a controllable change in doping efficiency, expressed in change of charge carrier concentration Δn, ranging between $+5.7 \times 10^{12}$ cm^{-2} and $+1.1 \times 10^{13}$ cm^{-2} was obtained, which was 50% higher in comparison with that obtained by F4-TCNQ applied by vapour deposition [32] and simultaneously fulfilled the above mentioned optical quality requirements. Nevertheless, a further improvement of the doping efficiency is desirable.

Another critical point related to the use of graphene and its doping, is the deposition and the patterning. Chemical vapor deposition (CVD) grown monolayer graphene can be transferred on different types of substrates [49]: rigid substrates (e.g. glass, quartz, silicon (Si), silicon dioxide (SiO_2)) and flexible substrates (e.g. PET) [50]. Depending on the desired application, we aim for either continuous graphene covering a large substrate surface (0.5 cm^2 – 1 m^2 range) [51] or smaller graphene domains covering specific structures (micro- to nanometer scale on e.g. optical waveguides or field effect transistors (FET)) [10–12,52]. As a consequence, the doping deposition technique needs to be adjusted, depending on its final application: chemical doping on large graphene areas is frequently applied by spin coating

View Article Online
DOI: 10.1039/C8TC03198C

(wet-chemical doping approach) or thermal evaporation [53], whereas localized dopant patterning still remains a niche [54]. The existing localized doping methods include different kinds of lithography and patterning techniques [55–57] for specific dopants (e.g. gold nanoparticles) which are not optimized for establishing optical-quality doping as we target here.

In this paper, we describe a new optical doping strategy based on surface transfer p-doping of graphene for optical applications and with the possibility for localized doping. The selected strategy should meet a predefined set of requirements. First, we aim for an optical-quality doping strategy revealing higher doping efficiencies than previously obtained with the F4-TCNQ/MEK dopant layer ($\Delta n > +2 \times 10^{13}$ cm^{-2}, with the aim to compete with the electrolyte-based graphene gating efficiencies). Secondly, the strategy should enable region-controlled micrometer-sized deposition on large scale substrates. We propose inkjet printing as a novel localized doping method to obtain lower light absorption in graphene-covered on-chip optical waveguides. The optical waveguides that we consider are Si waveguides, with Si being a primary material platform for on-chip data transmission at the telecom wavelength of 1550 nm [58]. Moreover, Si waveguides can be manufactured by means of Complementary Metal Oxide Semiconductor (CMOS) technology, enabling high-volume fabrication at low cost [58]. Silicon photonics, could potentially also be combined with silicon electronics creating hybrid integrated optoelectronic systems [59].

A first step towards such a doping strategy is the selection of a suitable p-type dopant, namely bis(trifluoromethanesulfonyl)amide (TFSA, $[CF_3SO_2]_2NH$) (figure 1A). We select TFSA because, to the best of our knowledge, it is the strongest p-type dopant currently existing, due its extremely strong acidity (pK_a = -11.9) yielding intrinsic strong electron accepting properties [33,42,60–62]. However, TFSA dissolved in e.g. nitromethane and subsequently spin coated onto graphene suffers from micrometer-sized clusters being formed [38]. Furthermore, optical transmission losses of at least 1% were described using perpendicularly incident light (for λ in the visible or infrared) on TFSA-deposited graphene [35,53,63]. Given its strong acidity, a final TFSA shortcoming is the water sensitivity although contradictory findings have been reported in literature on this matter [42,61].

View Article Online
DOI: 10.1039/C8TC03198C

With the aim to overcome the above-mentioned TFSA-related issues, we propose poly(2,2,3,3,4,4,5,5-octafluoropentyl methacrylate) (POFPMA, figure 1B) as polymer matrix for incorporating TFSA. The choice for POFPMA rather than PMMA (often used in graphene processing) originates from the inferior properties of both high (M_w = 350000 g/mol) and low (M_w = 6000 g/mol) molecular weight poly(methyl methacrylate) (PMMA, figure 1C) in terms of the solubility and the mechanical stability, respectively.

The present paper covers two interrelated parts. First, the chemical characterization of the TFSA/POFPMA dopant layer and the quantification of the doping efficiency for larger areas obtained through spin coating are described. The second part focusses on the spatially controlled deposition of the TFSA/POFPMA dopant through inkjet printing with a final application on graphene-covered waveguides.

View Article Online
DOI: 10.1039/C8TC03198C

2. Results and discussion

2.1 TFSA/POFPMA doping on graphene on top of flat Si samples by spin coating

2.1.1 Characterization of the spin coated TFSA/POFPMA layer

Acids are often used as p-doping molecules on graphene, due to their oxidizing effect; the acidic proton(s) can cause a charge transfer by extracting electrons from graphene [27,51,64,65]. We studied the doping effect of various acids in function of their acidity level (expressed in pK_a units) and used transferred graphene onto Si samples as substrate with a polished top side exhibiting a very high surface quality. We concluded that the p-doping effect increases with a higher acidity strength. The results are included in the supplementary information, figure S1. Since TFSA (figure 1A) is categorized as a super acid (pK_a = -11.9), it is a commonly used strong p-dopant which can moreover be easily applied by spin coating in e.g. nitromethane [42]. However, for the solvents used to date for TFSA on graphene, the spin coated deposition features particle formation [41] (figure 2A), which is detrimental for optical applications [66,67]. In addition, the spin coated TFSA deposition on graphene suffers from temporal instability when exposed to the atmosphere, due to its high sensitivity to humidity [42].

To counteract these shortcomings, we incorporated TFSA as active dopant molecule into a POFPMA polymer matrix (figure 1B) as PMMA could not fulfill the role as candidate matrix material (see introduction and further detailed below). Knowing that PMMA (figure 1C) is very often used as supporting layer for transferring graphene, we selected POFPMA as it is also a polymethacrylate in which the fluorine atoms in the side chains are likely to benefit the transparency due to the lower energy absorption bands of fluorine compared to hydrogen [68]. The matrix polymer POFPMA was used directly after synthesis without any further purification due to the absence of a solvent during the bulk polymerization. The molecular weight (M_w) of the synthesized POFPMA was determined at 3200 g/mol (with a polydispersity (Đ) of 1.99), the degradation temperature ($T_{d,95}$) at 243°C and the glass transition temperature (T_g) at 17°C. We anticipated that the low T_g-value of the bulk POFPMA will not impose any problems given the high surface energy of graphene, leading to an increased T_g of the obtained thin polymer films [69–71].

View Article Online
DOI: 10.1039/C8TC03198C

We noted that while using PMMA as a 10 w/v% in ethylacetate with a high molecular weight (M_w of 350000 g/mol) and a T_g of 105°C, typically used for transferring graphene, to incorporate the TFSA dopant, led to more clustered surfaces (RMS roughness of 2.4 nm/25 μm^2). PMMA with a lower molecular weight (M_w of 6000 g/mol), a T_g of 75°C and applied from a 20 w/v% in acetone though, resulted in a cracked layer after drying. We therefore concluded that POFPMA revealing a M_w of 3200 g/mol and a T_g of 17°C and applied from a 20 w/v% solution in acetone, offered a good compromise with its lower molecular weight sustaining good solubility thus guaranteeing a uniform film formation and its lower T_g enabling smoother surfaces to be obtained.

Optical microscopy analyses of the spin coated layers, consisting of TFSA (0 – 40 mM) and POFPMA (20 w/v %) in acetone onto graphene, revealed a uniform and cluster-free surface (figure 2B). Additionally, SEM images of the TFSA/POFPMA dopant layer are presented in the supplementary information (figure S2).

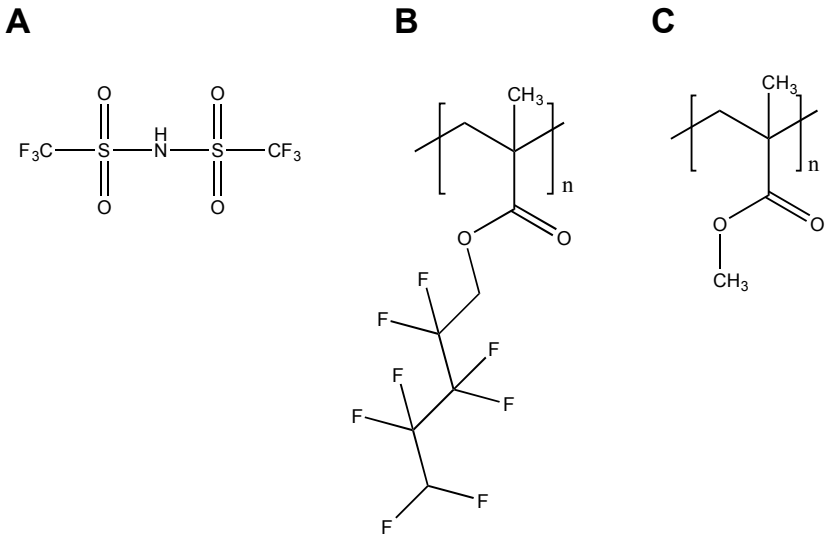

Figure 1. Chemical structures of (A) TFSA), (B) POFPMA and (C) PMMA. Additionally, the crystal structure of TFSA is presented with the carbon atoms represented by grey, fluorine atoms by green, hydrogen atom by white, nitrogen atom by blue, oxygen atoms by red and sulfur atoms by yellow colors.

View Article Online
DOI: 10.1039/C8TC03198C

The roughness of the spin coated TFSA/POFPMA layer was determined by atomic force microscopy (AFM). While a bare Si substrate exhibits a very high surface quality (figure 2D, RMS roughness of only 0.5 nm/25 μm^2), the roughness of the surface increased to 2.2 nm/25 μm^2 (figure 2E) after transferring graphene, due to the monolayer of carbon atoms containing PMMA residues [72]. After spin coating a TFSA/POFPMA layer onto the graphene, the roughness decreased to 0.4 nm/25 μm^2, corresponding with an optical quality of λ/1000 at a wavelength of 400 nm (figure 2F). Whereas the RMS roughness of the TFSA in nitromethane deposition was 14.9 nm/25 μm^2, the TFSA/POFPMA layer yielded an enhanced smoothness, even in comparison with the uncovered Si samples.

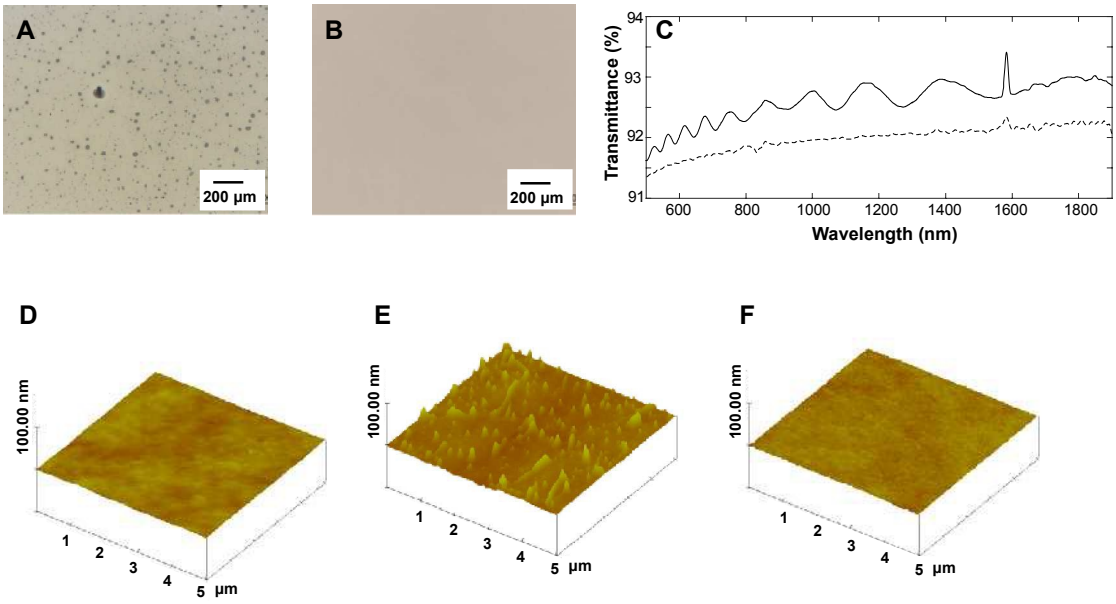

Figure 2. Analysis of the optical quality of the TFSA/POFPMA dopant layer: Optical microscopy image of (A) TFSA (20 mM) dissolved in nitromethane and (B) TFSA/POFPMA (20 mM TFSA and 20 w/v% POFPMA) dissolved in acetone, spin coated onto graphene. (C) Optical transmittance of a glass substrate (dashed line) and TFSA/POFPMA spin coated on glass (full line). AFM 3D surface plots of (D) a polished Si sample with a (E) transferred monolayer graphene on top and (F) additionally covered with a spin coated TFSA/POFPMA layer.

View Article Online
DOI: 10.1039/C8TC03198C

The homogeneity of the polymer layer was determined by X-ray photoelectron spectroscopy (XPS) measurements and is presented in table 1. The atoms corresponding to TFSA only (sulfur and nitrogen) were not detected due to the low concentrations present in the obtained layer (ranging from 0.75 – 40 mM TFSA). The small standard deviation clearly confirmed the good uniformity of the polymer matrix layer.

Table 1. XPS results of a bare graphene-covered Si substrate and a spin coated TFSA/POFPMA layer on a graphene-covered Si substrate (concentration TFSA = 20 mM). The table summarizes the average values and the corresponding standard deviations derived from measurements at three randomly selected positions on the surface.

	Monolayer graphene transferred on Si		TFSA/POFPMA spin coated on graphene	
Element	Average (%)	Std. Dev. (%)	Average (%)	Std. Dev. (%)
O	24.99	0.8	9.9	0.2
C	47.63	1.2	44.28	0.6
F	-	-	45.83	0.7
Si	24.63	0.6	-	-

The thickness of the spin coated layers as a function of the spin speed was determined by ellipsometry (see figure S3). At a spin speed of 5000 rounds per minute (rpm), a thickness around 2 µm was obtained for the TFSA/POFPMA layer. The latter thickness was high enough to ensure a stable and robust layer for future doping tests (see section 3.1.2).

Finally, the transparency of the TFSA/POFPMA layer was evaluated by optical transmission measurements (figure 2C). POFPMA is as PMMA a methacrylate-based polymer with additional fluorine atoms, POFPMA was expected to offer very high transparency. The transmission measurements confirmed that the spin coated layer hardly diminished (A < 0.05 %) the optical transmittance when coated onto a glass substrate. The oscillations and the slightly higher transmittance of the TFSA/POFPMA layer compared to the bare glass substrate are due to interference effects of the 2 µm thick polymer layer.

2.1.2 Doping of graphene with a spin coated TFSA/POFPMA layer

View Article Online
DOI: 10.1039/C8TC03198C

As TFSA was successfully incorporated in the POFPMA polymer layer featuring optical quality, as evidenced in section 3.1.1, we determined in a next step the doping efficiency of TFSA/POFPMA by spin coating the dopant layer on monolayer graphene provided by CVD growth and electrochemically transferred onto flat Si substrates. Graphene is characterized by important parameters such as the charge carrier concentration (n in cm^{-2}), the mobility (μ in $cm^2\ V^{-1}\ s^{-1}$) and the sheet resistance (Rs in Ω/sq). These electrical parameters were monitored and quantified via Hall effect measurements prior and after doping. Transferred CVD graphene itself features a slight p-doping with n of the order of +(2–6) x 10^{12} cm^{-2}. When applying additional p-doping, one expects to extract electrons from graphene, creating more holes in graphene, thus increasing the concentration of charge carriers while simultaneously decreasing the sheet resistance. Consequently, we expressed the doping efficiency in terms of the change in charge carrier concentration; $\Delta n = n_{after\ doping} - n_{before\ doping}$ (cm^{-2}) and the decrease in sheet resistance = $Rs_{after\ doping}$ / $Rs_{before\ doping}$ x 100 (%). TFSA concentrations ranging from 0 to 40 mM were applied in combination with POFPMA onto graphene. The obtained results are shown in figure 3 and table S1.

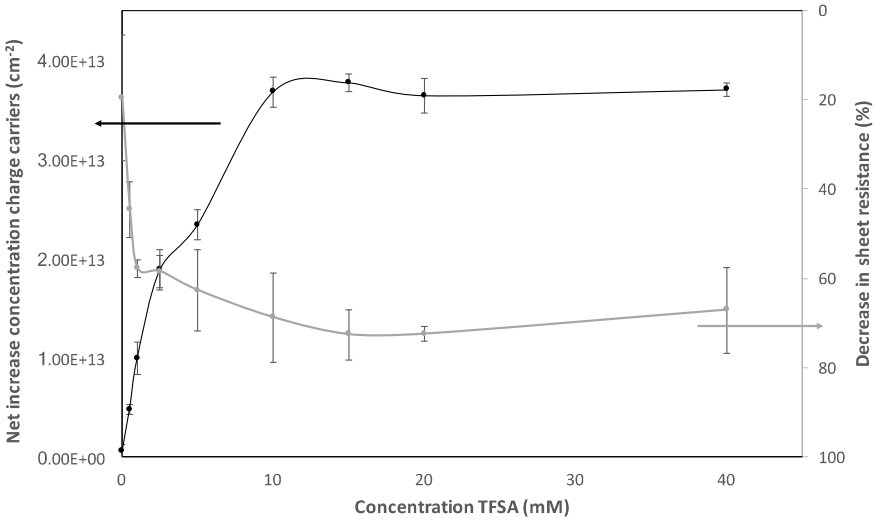

Figure 3. Change in charge carrier concentration (Δn in cm^{-2}, black line and left y-axis) and decreasing sheet resistance (%, grey line and right y-axis), starting from CVD grown graphene on copper followed by transfer to Si substrates and subsequent doping with a TFSA/POFPMA

View Article Online
DOI: 10.1039/C8TC03198C

layer, as a function of the TFSA concentration ranging from 0 to 40 mM. Each dopant solution is applied on three different samples.

For every dopant concentration applied, an increase in graphene doping was obtained with a positive Δn between +4.8 x 10^{12} and +3.8 x 10^{13} cm^{-2}, corresponding to a decrease in Fermi level of 0.13 and 0.55 eV, respectively. For the latter values, a starting Fermi level of -0.23 eV was calculated for the undoped graphene, so after doping we obtained a Fermi level of respectively, -0.36 eV and -0.78 eV, depending on the doping concentration applied. The maximal increase in charge carrier concentration was accompanied with a strong decrease in sheet resistance, resulting in a value of 37.5% of its initial value after doping, which ranges between 900 and 2000 Ω/sq. Although fluorine atoms are present in the POFPMA polymer in contrast to PMMA, pure POFPMA has a negligible doping effect of only Δn = +1.4 x 10^{12} cm^{-2}. TFSA incorporation highly augments the doping with an optimal effect at a TFSA concentration of 15 mM. Further increase of the TFSA concentrations leads to saturation of the doping effect due to stronger intermolecular repulsive forces of charged TFSA molecules [73] and an increasing capturing probability for freely moving holes in the graphene sheet due to the presence of more ionized attraction centers in the dopant layer [74]. This doping regime with a saturation mechanism above a specific concentration is similar to that of F4-TCNQ/MEK doping [48] and was also observed earlier on for TFSA doping [42]. In this way, we were able to dope graphene in a controllable manner without saturation when varying the TFSA concentration between 0 and 15 mM. Every concentration higher than 15 mM resulted in the maximum doping increase of almost +4 x 10^{13} cm^{-2}.

Although we obtained a doping efficiency up to Δn = +3.8 x 10^{13} cm^{-2} and a 72.5% decrease in the sheet resistance, we noted that spin coating of pure TFSA in nitromethane on graphene resulted in a higher doping efficiency [42]. The use of a POFPMA matrix, to guarantee the optical quality, diminishes the doping efficiency of TFSA, but, the net increase of Δn = +3.8 x 10^{13} cm^{-2} is in a range which is suitable to significantly and positively affect the optical properties of graphene at the common telecom wavelength of 1550 nm (see section 2.2.2). Not only the optical quality benefits from the use of the developed POFPMA matrix but also the stability is highly improved. Since TFSA reacts violently with water, the slightest environmental moisture causes a change in the observed doping effect. To overcome this instability, the spin coated POFPMA matrix serves as a protective layer; while the maximum

View Article Online
DOI: 10.1039/C8TC03198C

increase in charge carrier concentration was obtained after three days (the latter period was needed to set-in the maximum electron exchange from graphene to dopant layer and the waiting period to obtain the maximum doping efficiency was also notified with the use of the organic F4-TCNQ/MEK dopant layer [48]), a change of only 10% was noticed for a period of several months (figure S4). Compared to the previously reported TFSA doping experiments [35][38], the latter use of TFSA in POFPMA offered a significant increase in stability in function of time.

As an intermediate while important conclusion, TFSA embedded in the developed POFPMA polymer layer and applied through spin coating reveals to be a successful approach to apply TFSA as p-dopant for optical applications. The doping is controllable by using different concentrations TFSA mixed in POFPMA (20 w/v% in acetone) over a wide window, ranging from $\Delta n = +1.4 \times 10^{12}$ cm^{-2} to $+3.8 \times 10^{13}$ cm^{-2}.

In the following section, we will extend the above described and acquired knowledge of the TFSA/POFPMA doping method for localized application on a graphene-covered optical waveguide.

View Article Online
DOI: 10.1039/C8TC03198C

2.2 TFSA/POFPMA doping on a graphene-covered silicon waveguide

2.2.1 Characterization of inkjet printed TFSA/POFPMA deposition

TFSA/POFPMA dissolved in acetone served as an ideal dopant strategy to control graphene's Fermi level via spin coating when the dopant is deposited onto large graphene areas. However, when applying the dopant onto optical waveguides, it is an important advantage if the dopant deposition can be well localized at a precisely chosen position on the chip. Indeed, this allows doping different waveguides with different doping efficiencies e.g. by changing the dopant concentration used for various waveguides. Spin coating does not enable such a flexibility because it results in a total spreading of the dopant on the chip surface. Furthermore, whereas applying spin coating is straightforward on planar substrates, this is not necessarily the case for spin coating on photonic chips containing non-planarized waveguides (i.e. waveguides that 'stick out' from the substrate surface as we considered here). Therefore, when applying graphene on a waveguide, we selected inkjet printing as technique to deposit TFSA/POFPMA, enabling micrometer-sized local depositions starting from a liquid ink. Unfortunately, we could not apply the dopant composition optimized for spin coating conditions (TFSA/POFPMA (20 w/v%) in acetone) for the inkjet printing, due to the high vapor pressure of acetone [75] (30 kPa at 20°C). We therefore replaced acetone by the OFPMA monomer as solvent, which yielded a straightforward printable ink, exhibiting much structural similarity with the polymer material POFPMA itself. A concentration of 20 w/v% POFPMA in OFPMA was applied. Concentrations higher than the latter value could not be printed due to obstructions of the print nozzles.

When printing on a flat graphene sample, lined patterns were obtained as shown on the microscopy image in figure 4A. The width of the lines is 125 µm, regardless the number of printed layers. The obtained resolution confirmed inkjet printing as a promising tool to dope graphene with micro-scale precision on a photonic chip. Furthermore, when printing a three-layered TFSA/POFPMA line, we obtained a 3D-pattern. Its cross section, presented in figure 4B, clearly reveals the well-known 'coffee-ring' effect. This phenomenon occurs during drying of the droplets where an increased solvent evaporation rate towards the edges of the patterns lead to an accumulation of the material [76]. Nevertheless, the center of the printed line still possesses a height of 380 nm, which was sufficient to ensure good robustness and coverage level of the dopant deposition on the 220 nm high waveguide (see

View Article Online
DOI: 10.1039/C8TC03198C

section 2.2.2). Since the applied deposition technique is vastly different compared to spin coating, AFM measurements were executed to quantify the roughness of the printed patterns, resulting in a RMS roughness of 0.8 nm/25 μm^2 (shown in figure 4C). Despite the slight increase in the TFSA/POFPMA roughness for the printed TFSA/POFPMA deposition compared to the spin coated roughness (0.4 nm/25 μm^2), it still fulfills the objectives for optical-quality requirements (RMS roughness < 5 nm/25 μm^2), as stated in the introduction.

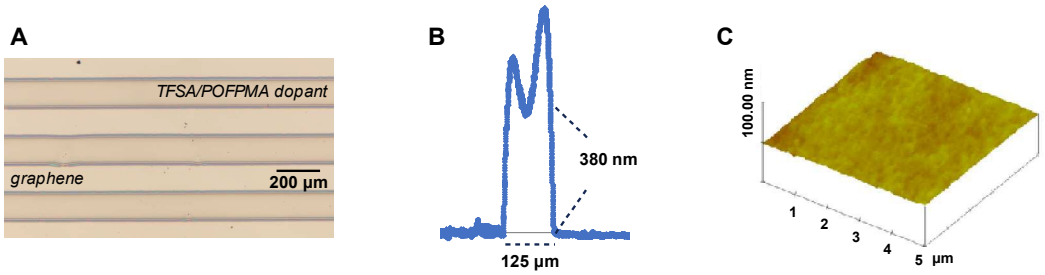

Figure 4. TFSA/POFPMA lines (3 layers) printed on graphene transferred on flat silicon (A), a cross section of a printed line (measured with stylus profilometry) (B) and an AFM 3D surface plot in the center of the printed dopant deposition (C).

We also verified the doping capability of the inkjet-printed TFSA/POFPMA dopant deposition on flat graphene-covered Si substrates. The characterization procedure has been as follows: we initially carried out Hall measurements on the flat graphene-covered sample prior to doping. Subsequently, we inkjet-printed several TFSA/POFPMA dopant lines (see figure 4A). and repeated the Hall measurements afterwards. We observed that the inkjet-printed dopant lines yielded an increase in charge carrier concentration and a decrease in sheet resistance, as we expected and which is in agreement with the trend observed for the spin coated doping strategy and presented in figure 3. It should be noted that, whereas the spin coated TFSA/POFPMA dopant layer caused a full coverage of the graphene surface, the inkjet printed dopant deposition only partially covered the graphene surface (see figure 4A, showing a zoom-in of three printed lines). We verified that the change in charge carrier concentration for the sample with the printed lines was proportional to the change in charge carrier concentration for the sample with the spin coated layer multiplied by the surface coverage of the printed lines. The data can be found in the supplementary information (figure S5 and table S2).

View Article Online
DOI: 10.1039/C8TC03198C

To complete the analysis of the printed TFSA/POFPMA dopant, we applied it to a photonic chip with Si waveguides to examine the influence of the TFSA/POFPMA deposition on the waveguides (without graphene) by performing optical transmission measurements prior and after TFSA/POFPMA deposition. The results have shown negligible transmission change for a length of 700 µm dopant deposition, indicating that TFSA/POFPMA has a negligible effect on the optical absorbance or scattering of the light through the waveguide.

2.2.2 Doping efficiency of TFSA/POFPMA on graphene-covered Si waveguides

After the confirmation of the doping capacity of the inkjet-printed dopant through Hall measurements, we continued by applying the TFSA/POFPMA dopant onto an SOI chip with straight Si waveguides covered with graphene over small distances, namely 100 µm, 200 µm and 300 µm graphene strip lengths on different sections of the chip. Since Hall measurements are challenging on graphene with dimensions of the order of 100 µm, we examined the doping efficiency with optical transmission measurements.

To assess the absorption induced by undoped graphene, the optical transmission of different graphene-covered Si waveguides was measured, without dopant. The transmission was characterized at the telecom wavelength of 1550 nm. In a second measurement, the optical transmission of the same waveguides was characterized, this time additionally covered with TFSA/POFPMA dopant applied by inkjet printing. Due to a relatively slower drying process of the printed deposition in comparison with the spin coated deposition, we applied a TFSA concentration of 40 mM. The latter concentration is situated in the saturated regime of the doping efficiency (see figure 3), to ensure effective doping. An example of the chip lay-out, for the region with a 100 µm graphene strip length after doping is presented in figure 5. Four waveguides, indicated with number 1-4, can be observed, which were all measured in the first and second transmission measurements. Additionally, the graphene region covers three waveguides (2-4) while the dopant only covers waveguides 4 as can be seen in figure 5. Whereas the waveguide with number 1 was the reference waveguide (without graphene and dopant), the waveguide 4 was our target waveguide where graphene and later doping was applied. This waveguide has a width of 0.7 µm. Meanwhile, we executed reference measurements on waveguide 1 during the first and second optical transmission measurements and observed a similar optical insertion loss, as expected. Therefore, we

View Article Online
DOI: 10.1039/C8TC03198C

could compare the obtained results of both measuring cycles. Similar experimental chip lay-outs and measurements were performed for the other sections on the same chip where similar waveguides with the same dimensions have been fabricated but that were covered with 200 µm and 300 µm graphene strip length, respectively.

In figure 6 the optical transmissions are shown for the waveguides 4 with a width of 0.7 µm and with varying graphene lengths on top, measured when the graphene is undoped and when the graphene is doped with TFSA/POFPMA. We observed that the loss induced by the *undoped* graphene was equal to 7.38 dB per 100 µm graphene length (for the TE-polarized waveguide mode). This value is extracted from the slope of the grey line in figure 6A. It is clear from these measurements that the insertion loss has a linear relation to the graphene length, as expected [12]. For the *doped* graphene-covered Si waveguides, the induced loss was decreased: it became 3.16 dB per 100 µm graphene length (extracted from the slope of the black line in figure 6A). Hence the doping-induced improvement in optical transmission for the waveguides was 4.22 dB per 100 µm graphene length, as shown in figure 6B. The latter clearly revealed the linear correlation of the enhanced transmission with the graphene length.

To the best of our knowledge, these are the first reported experiments based on an inkjet printed dopant on graphene-covered waveguides, with promising results in view of the strong average transmission increase around 4.22 dB per 100 µm graphene length as compared to undoped graphene-covered waveguides.

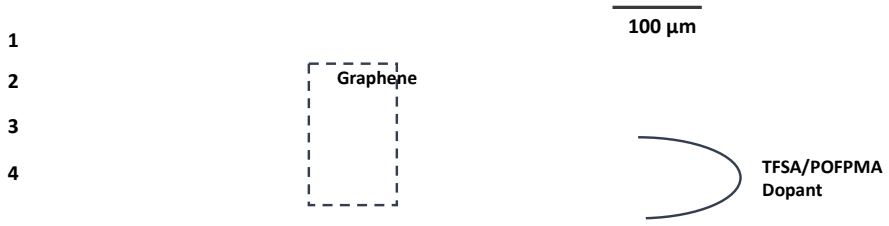

Figure 5. An optical microscopy image of a section of the optical chip. Graphene with a strip length of 100 µm was on top of the waveguides (indicated with the dotted line rectangular shape) and TFSA/POFPMA dopant was deposited via inkjet printing. Four waveguides are also indicated with number 1-4.

View Article Online
DOI: 10.1039/C8TC03198C

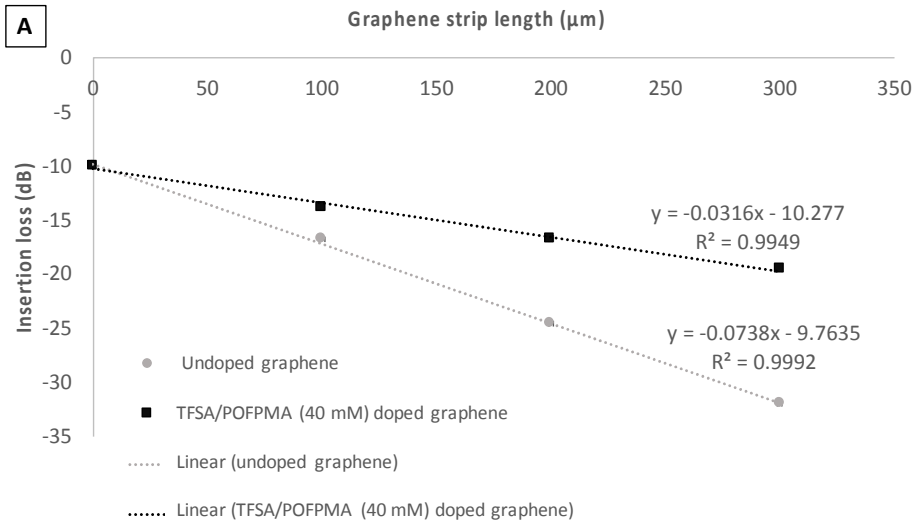

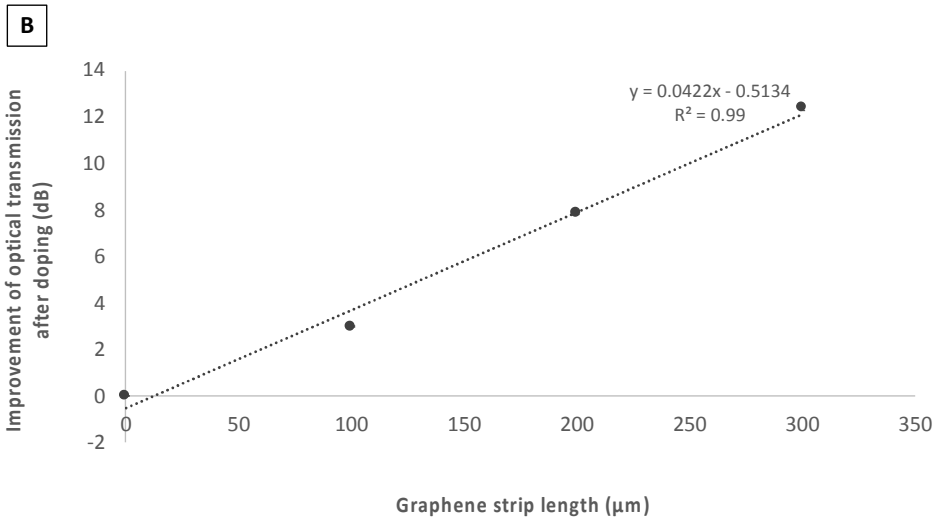

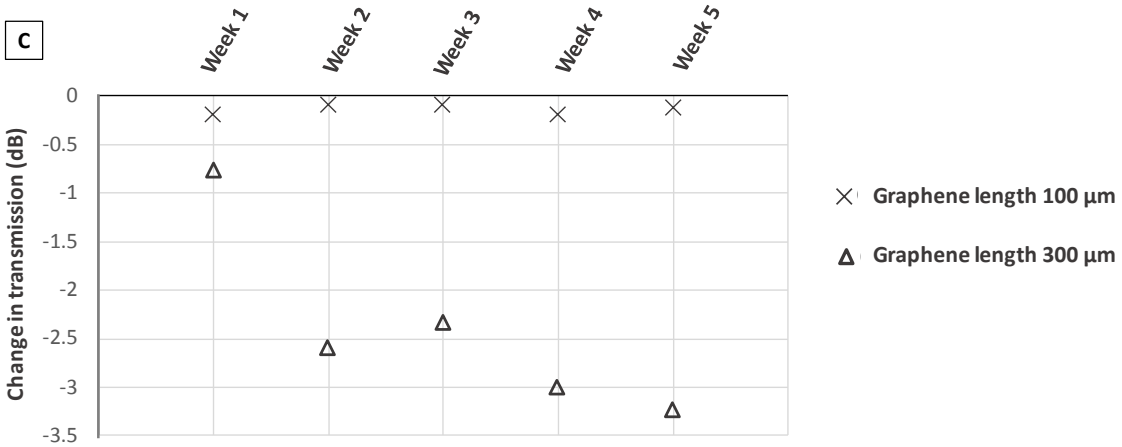

View Article Online
DOI: 10.1039/C8TC03198C

Figure 6. (A) The optical transmission at a wavelength of 1550 nm, measured for graphene-covered waveguides (with a width of 0.7 µm) without and with TFSA/POFPMA (40 mM) dopant (grey and black, respectively) and (B) the improvement in transmission for doped graphene-covered Si waveguides in function of graphene strip length. (C) Stability measurement by monitoring the change in optical transmission in function of time (averaged per week, with graphene lengths of 100 and 300 µm). The error on the optical transmission measurements was less than 5%.

The stability of the printed deposition was monitored over a period of several weeks. The change of the optical transmission of the doped graphene-covered waveguides is presented in figure 6C. The originally obtained transmission values were guaranteed for that period of time for a graphene length of 100 µm. For a graphene strip length of 300 µm however, the doping-induced transmission increase started to diminish after some weeks (around 3 dB transmission decrease after 5 weeks, which is still a modest decrease compared to the starting value in figure 6A). The doping stability of the inkjet printed TFSA/POFPMA dopant was less compared to that of the spin coated deposition. The main reason for this significant difference is the thickness of the deposition which is 5 times less for the inkjet-printed deposition compared to the spin coated layers. In addition, the surface-volume ratio is also higher for the printed deposition, which enlarges the exposure to a humid environment for the TFSA molecules.

Finally, we calculated the theoretical doping level from the obtained optical transmission data via MODE simulations (see Experimental Methods in Supplementary Information). According to the simulations, the final Fermi level after doping graphene should be around -0.45 eV for an increase in linear optical transmission of 4.22 dB per 100 µm graphene on a Si-waveguide (see experimental results above). This corresponds to an increase (in absolute value) of the Fermi level of 0.22 eV, when -0.23 eV was determined as initial Fermi level. The 0.22 eV increase is lower than the change in Fermi levels obtained for graphene doped with spin coated TFSA/POFPMA layers (a maximum change of the Fermi level of 0.53 eV for a TFSA concentration of 40 mM was described in section 3.1.2). Probably, both the volume of the doping layer and the deposition method with another solvent (acetone compared to liquid OFPMA) are the reasons underlying these findings. However, the increase in optical

View Article Online
DOI: 10.1039/C8TC03198C

transmission of 4.22 dB per 100 µm of graphene length is remarkable and promising for future optical applications.

3. Conclusion

The present work described an optical doping strategy for graphene, based on a TFSA/POFPMA layer. The developed dopant consists of TFSA as super acid and thus a strong p-type dopant, and POFPMA as polymer matrix. The latter was applied to improve, on the one hand the optical quality, and on the other hand the environmental stability over time. The former optical quality was confirmed by a low surface roughness of only 0.4 nm/25 μm^2 and a very high transparency (A < 0.05%) over the wavelength range between 500 and 1900 nm.

TFSA/POFPMA can be applied in a straightforward fashion onto large area graphene via spin coating. We quantified the doping efficiency by monitoring graphene's electrical parameters through Hall measurements: an increase of charge carrier concentration (holes) between +4.8 x $10^{12}cm^{-2}$ and +3.8 x $10^{13}cm^{-2}$ was observed, for varying TFSA concentrations between 0 and 40 mM.

Furthermore, the TFSA/POFPMA dopant could also be deposited in localized micrometer-sized patterns using inkjet printing. A three-layer thick print line featured sufficient height to cover a 220 nm high waveguide and the printed line also offered a low surface roughness of only 0.8 nm/25 μm^2, without inducing any additional propagation losses. The optical transmission was strongly improved when doping a graphene-covered waveguide: a transmission increase of 4.22 dB/100 µm graphene length at a wavelength of 1550 nm was obtained. Both deposition methods showed significant stability of the doping efficiency as a function of time for a period of at least five weeks.

The herein reported tests were the first in their kind using inkjet-printed dopants and allow enhanced optical transmission of graphene-covered waveguides. The developed methodology will be very promising when exploiting graphene for future optical and photonic applications.

Acknowledgement

This work was supported by ERC-FP7/2007–2013 grant 336940, EU-FET GRAPHENICS (grant agreement no. 618086), EU-FP7 Graphene Flagship (grant agreement no. 604391), the Polish

View Article Online
DOI: 10.1039/C8TC03198C

National Science Centre UMO-2013/09/N/ST5/02481, VUB-OZR and, Methusalem. M.K and N.V. wish to acknowledge partial financial support by Research Foundation - Flanders (FWO) in the frame of the EOS Project G0F6218N (EOS ID 30467715).

4. References

1. Novoselov, K.S., Geim, A.K., Morozov, S.V., et al. (2004) Electric field effect in atomically thin carbon films. *Science*, **306**, 666–669.
2. Castro Neto, A.H., Peres, N.M.R., Novoselov, K.S., et al. (2009) The electronic properties of graphene. *Rev. Mod. Phys.*, **81** (1), 109–162.
3. Morozov, S. V, Novoselov, K.S., Katsnelson, M.I., et al. (2008) Giant Intrinsic Carrier Mobilities in Graphene and Its Bilayer. *Phys. Rev. Lett.*, **100** (1), 16602.
4. Lee, C., Wei, X., Kysar, J.W., and Hone, J. (2008) Measurement of the Elastic Properties and Intrinsic Strength of Monolayer Graphene. *Science*, **321**, 385–388.
5. Bonaccorso, F., Sun, Z., Hasan, T., and Ferrari, A.C. (2010) Graphene photonics and optoelectronics. *Nat. Photonics*, **4** (9), 611–622.
6. Bao, Q., and Loh, K.P. (2012) Graphene photonics, plasmonics, and broadband optoelectronic devices. *ACS Nano*, **6** (5), 3677–94.
7. Wang, J., and Hu, X. (2017) *Graphene Materials - Advanced Applications - Chapter 8: Graphene-Enhanced Optical Signal Processing*.
8. Margulis, V.A., Muryumin, E.E., and Gaiduk, E.A. (2017) A theory for non-degenerate four-wave mixing in doped graphene. *Phys. B Condens. Matter*, **509** (September 2016), 70–75.
9. Hendry, E., Hale, P.J., Moger, J., et al. (2010) Coherent nonlinear optical response of graphene. *Phys. Rev. Lett.*, **105** (9), 1–4.
10. Vermeulen, N., Castello-Lurbe, D., Cheng, J., et al. (2016) Negative Kerr Nonlinearity of Graphene as seen via Chirped-Pulse-Pumped Self-Phase Modulation. *Phys. Rev. Appl.*, **6** (4).
11. Vermeulen, N., Castello-Lurbe, D., Khoder, M., et al. (2018) Graphene's nonlinear-optical physics revealed through exponentially growing self-phase modulation. *Nat. Commun.*, **9** (1).
12. Van Erps, J., Ciuk, T., Pasternak, I., et al. (2015) Laser ablation- and plasma etching-based patterning of graphene on silicon-on-insulator waveguides. *Opt. Express*, **23**

View Article Online
DOI: 10.1039/C8TC03198C

(20), 26639.

13. Li, H., Anugrah, Y., Koester, S.J.S., and Li, M. (2012) Optical absorption in graphene integrated on silicon waveguides. *Appl. Phys. Lett.*, **101** (111110), 1–5.
14. Cheng, J.L., Vermeulen, N., and Sipe, J.E. (2015) Third-order nonlinearity of graphene: Effects of phenomenological relaxation and finite temperature. *Phys. Rev. B - Condens. Matter Mater. Phys.*, **91** (23).
15. Yu, S., Wu, X., Wang, Y., et al. (2017) 2D Materials for Optical Modulation : Challenges and Opportunities. *Adv. Mater.*, **29** (14).
16. Guo, B., Fang, L., Zhang, B., and Gong, J.R. (2011) Graphene Doping: A Review. *Insciences J.*, **1** (2), 80–89.
17. Liu, H., Liu, Y., and Zhu, D. (2011) Chemical doping of graphene. *J. Mater. Chem.*, **21** (10), 3335.
18. Pham, V.P., Kim, K.H., Jeon, M.H., et al. (2015) Low damage pre-doping on CVD graphene/Cu using a chlorine inductively coupled plasma. *Carbon*, **95**, 664–671.
19. Markevich, A., Kurasch, S., Lehtinen, O., et al. (2016) Electron beam controlled covalent attachment of small organic molecules to graphene. *Nanoscale*, **8** (5), 2711–9.
20. Xu, K., Lu, H., Kinder, E.W., et al. (2017) Monolayer Solid-State Electrolyte for Electric Double Layer Gating of Graphene Field-Effect Transistors. *ACS Nano*, **11** (6), 5453–5464.
21. Das, A., Pisana, S., Chakraborty, B., et al. (2008) Monitoring dopants by Raman scattering in an electrochemically top-gated graphene transistor. *Nat. Nanotechnol.*, **3** (4), 210–215.
22. Wang, H.I., Braatz, M.-L., Richter, N., et al. (2017) Reversible Photochemical Control of Doping Levels in Supported Graphene. *J. Phys. Chem. C*, **121**, 4083–4091.
23. Wang, H., Wu, Y., Cong, C., et al. (2010) Hysteresis of electronic transport in graphene transistors. *ACS Nano*, **4** (12), 7221–7228.
24. Kim, Y., Rye, J., Park, M., et al. (2014) Vapor-Phase Molecular Doping of Graphene for High-Performance Transparent Electrodes. *ACS Nano*, **8** (1), 868–874.
25. Pirkle, A., Chan, J., Venugopal, A., et al. (2011) The effect of chemical residues on the physical and electrical properties of chemical vapor deposited graphene transferred to SiO2. *Appl. Phys. Lett.*, **99** (12), 2–5.

View Article Online
DOI: 10.1039/C8TC03198C

26. Jeong, H.J., Kim, H.Y., Jeong, S.Y., et al. (2014) Improved transfer of chemical-vapor-deposited graphene through modification of intermolecular interactions and solubility of poly(methylmethacrylate) layers. *Carbon*, **66**, 612–618.

27. Graupner, R., Abraham, J., Vencelová, A., et al. (2003) Doping of single-walled carbon nanotube bundles by Brønsted acids. *Phys. Chem. Chem. Phys.*, **5** (24), 5472–5476.

28. Krajewska, A., Oberda, K., Azpeitia, J., et al. (2016) Influence of Au doping on electrical properties of CVD graphene. *Carbon*, **100**, 625–631.

29. Chen, Z., Santoso, I., Wang, R., et al. (2010) Surface transfer hole doping of epitaxial graphene using MoO3 thin film. *Appl. Phys. Lett.*, **96** (21), 213104.

30. Kim, S., Shin, S., Kim, T., et al. (2017) A reliable and controllable graphene doping method compatible with current CMOS technology and the demonstration of its device applications. *Nanotechnology*, **28**, 175710.

31. Ji, Q., Shi, L., Zhang, Q., et al. (2016) VOx effectively doping CVD-graphene for transparent conductive films. *Appl. Surf. Sci.*, **387**, 51–57.

32. Coletti, C., Riedl, C., Lee, D.S., et al. (2010) Charge neutrality and band-gap tuning of epitaxial graphene on SiC by molecular doping. *Phys. Rev. B*, **81** (23), 235401.

33. Kim, D., Lee, D., Lee, Y., and Jeon, D.Y. (2013) Work-function engineering of graphene anode by bis(trifluoromethanesulfonyl)amide doping for efficient polymer light-emitting diodes. *Adv. Funct. Mater.*, **23** (40), 5049–5055.

34. Bausi, F., Schlierf, A., Treossi, E., et al. (2015) Thermal treatment and chemical doping of semi-transparent graphene films. *Org. Electron. physics, Mater. Appl.*, **18** (2), 53–60.

35. Shin, D.H., Jang, C.W., Kim, J.H., et al. (2017) Enhancement of efficiency and long-term stability in graphene/Si-quantum-dot heterojunction photodetectors by employing bis(trifluoromethanesulfonyl)-amide as a dopant for graphene. *J. Mater. Chem. C*, **5** (48), 12737–12743.

36. Han, T.H., Kwon, S.J., Li, N., et al. (2016) Versatile p-Type Chemical Doping to Achieve Ideal Flexible Graphene Electrodes. *Angew. Chemie - Int. Ed.*, **798**, 6197–6201.

37. Kwon, K.C., Choi, K.S., and Kim, S.Y. (2012) Increased work function in few-layer graphene sheets via metal chloride Doping. *Adv. Funct. Mater.*, **22** (22), 4724–4731.

38. Song, Y., Fang, W., Hsu, A.L., and Kong, J. (2014) Iron (III) chloride doping of CVD graphene. *Nanotechnology*, **25** (39), 395701.

View Article Online
DOI: 10.1039/C8TC03198C

39. Wehenkel, D.J., Bointon, T.H., Booth, T., et al. (2015) Unforeseen high temperature and humidity stability of FeCl3 intercalated few layer graphene. *Sci. Rep.*, **5**, 7609.

40. Kim, K.K., Reina, A., Shi, Y., et al. (2010) Enhancing the conductivity of transparent graphene films via doping. *Nanotechnology*, **21** (28), 285205.

41. Song, Y., Fang, W., Brenes, R., and Kong, J. (2015) Challenges and opportunities for graphene as transparent conductors in optoelectronics. *Nano Today*, **10** (6), 681–700.

42. Tongay, S., Berke, K., Lemaitre, M., et al. (2011) Stable hole doping of graphene for low electrical resistance and high optical transparency. *Nanotechnology*, **22**, 425701.

43. Kang, M.H., Milne, W.I., and Cole, M.T. (2016) Temporal Stability of Metal-Chloride-Doped Chemical-Vapour-Deposited Graphene. *ChemPhysChem*, **17** (16), 2545.

44. Jang, C.W., Kim, J.M., Kim, J.H., et al. (2015) Degradation reduction and stability enhancement of p-type graphene by RhCl3 doping. *J. Alloys Compd.*, **621**, 1–6.

45. Iqbal, M.Z., Iqbal, M.W., Khan, M.F., and Eom, J. (2015) Ultraviolet-light-driven doping modulation in chemical vapor deposition grown graphene. *Phys. Chem. Chem. Phys.*, **7** (32), 20551–20556.

46. Tiberj, a, Paillet, M., Landois, P., et al. (2013) Reversible optical doping of graphene. *Sci. Rep.*, **3**, 1–23.

47. Hornett, S.M., Heath, M., Horsell, D.W., and Hendry, E. (2014) Optically induced oxygen desorption from graphene measured using femtosecond two-pulse correlation. *Phys. Rev. B - Condens. Matter Mater. Phys.*, **90** (8), 1–5.

48. Misseeuw, L., Krajewska, A., Pasternak, I., et al. (2016) Optical-quality controllable wet-chemical doping of graphene through a uniform, transparent and low-roughness F4-TCNQ/MEK layer. *RSC Adv.*, **6** (106), 104491–104501.

49. Kang, J., Shin, D., Bae, S., and Hong, B.H. (2012) Graphene transfer: key for applications. *Nanoscale*, **4**, 5527–5537.

50. Verma, V.P., Das, S., Lahiri, I., and Choi, W. (2010) Large-area graphene on polymer film for flexible and transparent anode in field emission device. *Appl. Phys. Lett.*, **96** (20), 2008–2011.

51. Bae, S., Kim, H., Lee, Y., et al. (2010) Roll-to-roll production of 30-inch graphene films for transparent electrodes. *Nat. Nanotechnol.*, **5** (8), 574–578.

52. Wang, X.R., and Dai, H.J. (2010) Etching and narrowing of graphene from the edges. *Nat. Chem.*, **2** (8), 661–665.

View Article Online
DOI: 10.1039/C8TC03198C

53. Oh, J.S., Kim, K.N., and Yeom, G.Y. (2014) Graphene Doping Methods and Device Applications. *J. Nanosci. Nanotechnol.*, **14**, 1120–1133.

54. Velasco, J., Ju, L., Wong, D., et al. (2016) Nanoscale Control of Rewriteable Doping Patterns in Pristine Graphene/Boron Nitride Heterostructures. *Nano Lett.*, **16** (3), 1620–1625.

55. Huh, S., Park, J., Kim, K.S., et al. (2011) Selective n-type doping of graphene by photo-patterned gold nanoparticles. *ACS Nano*, **5** (5), 3639–3644.

56. Zhou, X., He, S., Brown, K.A., et al. (2013) Locally altering the electronic properties of graphene by nanoscopically doping it with rhodamine 6G. *Nano Lett.*, **13** (4), 1616–1621.

57. Bellido, E., Ojea-Jiménez, I., Ghirri, A., et al. (2012) Controlled positioning of nanoparticles on graphene by noninvasive AFM lithography. *Langmuir*, **28** (33), 12400–12409.

58. Thomson, D., Zilkie, A., Bowers, J.E., et al. (2016) Roadmap on silicon photonics. *J. Opt.*, **18** (7), 1–20.

59. Wang, X., Zhuang, X., Yang, S., et al. (2015) High Gain Submicrometer Optical Amplifier at Near-Infrared Communication Band. *Phys. Rev. Lett.*, **115** (2), 1–6.

60. Kütt, A., Rodima, T., Saame, J., et al. (2011) Equilibrium acidities of superacids. *J. Org. Chem.*, **76** (2), 391–395.

61. Foropoulos Jr, J., and DesMarteau, D.D. (1984) Synthesis, properties, and reactions of bis ((trifluoromethyl) sulfonyl) imide,(CF3SO2) 2NH. *Inorg. Chem.*, **23** (23), 3720–3723.

62. Miao, X., Tongay, S., Petterson, M.K., et al. (2012) High Efficiency Graphene Solar Cells by Chemical Doping. *Nano Lett.*, **12**, 6–11.

63. Tongay, S., Berke, K., Lemaitre, M., et al. (2011) Stable hole doping of graphene for low electrical resistance and high optical transparency. *Nanotechnology*, **22** (42), 425701.

64. Tantang, H., Ong, J.Y., Loh, C.L., et al. (2009) Using oxidation to increase the electrical conductivity of carbon nanotube electrodes. *Carbon*, **47** (7), 1867–1870.

65. Stergiou, A., Liu, Z., Xu, B., et al. (2016) Individualized p-Doped Carbon Nanohorns. *Angew. Chemie - Int. Ed.*, **55** (35), 10468–10472.

66. Han, T.-H., Lee, Y., Choi, M.-R., et al. (2012) Extremely efficient flexible organic light-emitting diodes with modified graphene anode. *Nat. Photonics*, **6** (2), 105–110.

View Article Online
DOI: 10.1039/C8TC03198C

67. Hyesung, P., Rowehl, J.A., Ki Kang, K., et al. (2010) Doped graphene electrodes for organic solar cells. *Nanotechnology*, **21**.

68. Koike, Y., and Koike, K. (2011) Progress in low-loss and high-bandwidth plastic optical fibers. *J. Polym. Sci. Part B Polym. Phys.*, **49** (1), 2–17.

69. Fryer, D.S., Fryer, D.S., Peters, R.D., et al. (2001) Dependence of the Glass Transition Temperature of Polymer Films on Interfacial Energy and Thickness. *Macromolecules*, **34**, 5627–5634.

70. van Engers, C.D., Cousens, N.E.A., Babenko, V., et al. (2017) Direct Measurement of the Surface Energy of Graphene. *Nano Lett.*, **17** (6), 3815–3821.

71. Keddie, J., Jones, , and A. Cory, R. (1994) Interface and surface effects on the glass-transition temperature in thin polymer films. *Faraday Discuss.*, **98**, 219-.

72. Matsumae, T., Koehler, A.D., Suga, T., and Hobart, K.D. (2016) A Scalable Clean Graphene Transfer Process Using Polymethylglutarimide as a Support Scaffold. *J. Electrochem. Soc.*, **163** (6), E159–E161.

73. Tian, X., Xu, J., and Wang, X. (2010) Band gap opening of bilayer graphene by F4-TCNQ molecular doping and externally applied electric field. *J. Phys. Chem. B*, **114**, 11377–11381.

74. Tietze, M.L., Pahner, P., Schmidt, K., et al. (2015) Doped organic semiconductors: Trap-filling, impurity saturation, and reserve regimes. *Adv. Funct. Mater.*, **25** (18), 2701–2707.

75. Taylor, R.S., and Smith, L.B. (1922) The vapor pressures, densities and some derived quantities for ether at low temperatures. *J. Am. Chem. Soc.*, **44** (11), 2450–2463.

76. Derby, B. (2010) Inkjet Printing of Functional and Structural Materials: Fluid Property Requirements, Feature Stability, and Resolution. *Annu. Rev. Mater. Res.*, **40** (1), 395–414.